Broadband infrared supercontinuum generation in hexagonal-lattice tellurite photonic crystal fiber with dispersion optimized for pumping near 1560 nm

Klimczak, Mariusz; Stepniewski, Grzegorz; Bookey, Henry; Szolno, Agnieszka; Stepien, Ryszard; Pysz, Dariusz; Kar, Ajoy Kumar; Waddie, Andrew John; Taghizadeh, Mohammad Reza; Buczynski, Ryszard

Published in:
Optics Letters

DOI:
10.1364/OL.38.004679

Publication date:
2013

Broadband infrared supercontinuum generation in hexagonal-lattice tellurite photonic crystal fiber with dispersion optimized for pumping near 1560 nm

Mariusz Klimczak,[1,*] Grzegorz Stepniewski,[1,3] Henry Bookey,[2] Agnieszka Szolno,[1] Ryszard Stepien,[1] Dariusz Pysz,[1] Ajoy Kar,[2] Andrew Waddie,[2] Mohammad R. Taghizadeh,[2] and Ryszard Buczynski[1,3]

[1]*Department of Glass, Institute of Electronic Materials Technology, Wolczynska 133, 01-919 Warsaw, Poland*

[2]*School of Engineering and Physical Sciences, Heriot-Watt University, Edinburgh EH14 4AS, Scotland, UK*

[3]*Faculty of Physics, University of Warsaw, Pasteura 7, 02-093 Warsaw, Poland*

**Corresponding author: mariusz.klimczak@itme.edu.pl*

Received August 9, 2013; revised October 1, 2013; accepted October 4, 2013; posted October 7, 2013 (Doc. ID 195427); published November 8, 2013

We report on supercontinuum generation (SG) in a hexagonal lattice tellurite photonic crystal fiber (PCF). The fiber has a regular lattice with a lattice constant $\Lambda = 2$ μm, linear filling factor $d/\Lambda = 0.75$, and a solid core 2.7 μm in diameter. Dispersion, calculated from scanning electron microscope (SEM) image of drawn fiber, has zero dispersion wavelength (ZDW) at 1410 and 4236 nm with a maximum of 193 ps/nm/km at 2800 nm. Under pumping with 150 fs/36 nJ/1580 nm pulses, supercontinuum spectrum in a bandwidth from 800 nm to over 2500 nm was observed in a 2 cm long PCF sample, which is comparable to results reported for suspended core tellurite PCFs pumped at wavelengths over 1800 nm. Measured spectrum is analyzed numerically with good agreement, and observed spectral broadening is interpreted. To our best knowledge, tellurite glass, regular lattice PCFs for successful SG in this bandwidth have not been reported before.

OCIS codes: (320.6629) Supercontinuum generation; (190.4370) Nonlinear optics, fibers; (060.5295) Photonic crystal fibers.

http://dx.doi.org/10.1364/OL.38.004679

Tellurite glass photonic crystal fibers (PCFs) offer a huge potential for broadband supercontinuum generation (SG) with bandwidths of 4000 nm demonstrated by Domachuk *et al.* in suspended core tellurite fibers (SC-PCFs) pumped around 1500–1600 nm, with 8 dB/m losses and sub-centimeter length of PCF [1]. Savelii *et al.* demonstrated tellurite SC-PCFs, first with 2 dB/m loss, then with a remarkable 0.1 dB/m loss [2,3], in which 840–3000 nm supercontinuum was recorded in PCFs as long as 50 cm. SG in tellurite SC-PCFs, mostly under pumping with Yb or Er wavelengths, has been reported by other groups as well [4,5]. SG in fibers with other types of photonic structure is not so common. 900–2500 nm bandwidths were reported in large-mode-area tellurite PCF under 150 fs pumping at 2150 nm [6] and in a hybrid tellurite-chalcogenide PCF under 1850 nm/180 fs pulses [7]. Regular lattice PCFs made of tellurite glasses are challenging because multiple thermal processing in drawing promotes recrystallization. On the other hand, it enables broad control of both dispersion and waveguide losses of guided modes. We recently reported tellurite glass synthesis and drawing of regular-lattice PCFs using a stack-and-draw method [8,9]. We also demonstrated narrow SG spectra in these PCFs under 800 nm pumping [10]. In this work, we present SG in a new, regular hexagonal-lattice tellurite PCF. SG bandwidth obtained under 1580 nm pumping was comparable with results reported for SC-PCFs under pumping at wavelengths exceeding 1800 or 2000 nm [6,7]. The demonstrated PCF shows reasonable attenuation of 6.2 dB/m at 1550 nm. To our best knowledge, this is the first regular lattice tellurite PCF successfully drawn, which enables SG under pumping with 1.5 μm wavelengths typical to relatively low-cost femtosecond Er^{3+} fiber lasers. Spectrum obtained in our PCF was reconstructed by a numerical model [11] with good agreement, enabling identification of broadening processes and discussion of their dynamics.

Fabricated PCF was drawn at the Institute of Electronic Materials Technology from an in-house synthesized tellurite glass labeled TWPN/I/6. Molar composition and rheological properties of glass used in this work are discussed in detail in our previous work [8]. The glass was adequate for multiple thermal processing without recrystallization, and the fiber was drawn using the stack-and-draw method. The fiber, shown with a guided mode in Fig. 1, has a 120 μm outer diameter. The hexagonal photonic structure is 23 μm in diagonal, the lattice constant is $\Lambda = 2$ μm, linear filling factor $d/\Lambda = 0.75$, and a solid core has 2.7 μm diameter. Fiber core has a very regular, circular geometry, which should result in negligible birefringence. Calculated birefringence of this fiber was below 10^{-6}. During spectrum measurements, input polarization was nevertheless rotated in order to optimize the supercontinuum bandwidth. Measured attenuation of our bulk tellurite glass

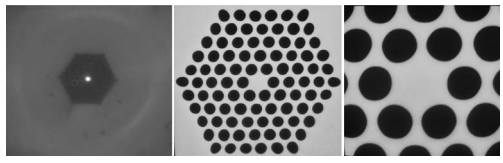

Fig. 1. Microstructure of fabricated tellurite PCF: large picture of photonic structure close-up with propagating mode as seen in a CCD camera, and SEM images of photonic structure.

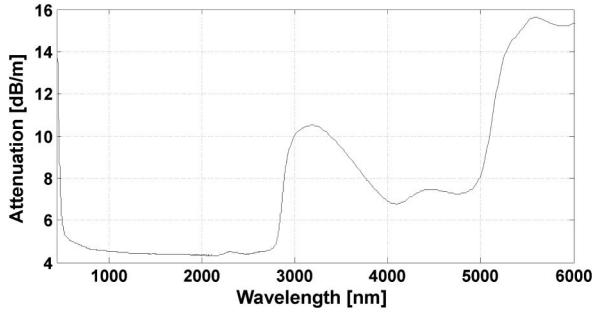

Fig. 2. Attenuation of tellurite glass used for fiber drawing. Attenuation of drawn PCF, measured at 1550 nm, was 6.2 dB/m.

is shown in Fig. 2. For most of the spectral area covered by obtained supercontinuum spectrum in this work, it stays under 5 dB/m, and attenuation measured in the drawn fiber at 1550 nm was at the level of 6.2 dB/m. Wavelength-dependent fiber loss used later in the modeling was therefore scaled up accordingly. Increase of attenuation around 3000 nm is related to content of OH ions. The dispersion profile shown in Fig. 3, calculated from scanning electron microscope (SEM) image of the drawn fiber, has zero dispersion wavelength (ZDW) at 1410 and 4236 nm with a maximum of 193 ps/nm/km at 2800 nm. Calculated effective mode area at pump wavelength was 3.0 μm^2 and was confirmed against experimental results (Fig. 1). For a measured nonlinear refractive index of our glass $n_2 = 18 \times 10 - 20$ m^2/W [11], this value yields nonlinear coefficient $\gamma = 238.6$ W^{-1} km^{-1}. The pump source was a Ti:sapphire-pumped OPA system (Tsunami/Splitfire, Spectra Physics) generating 150 fs pulses with 1 kHz repetition rate in the range of 1000–1600 nm. Pump pulse energy was limited with a gradient filter down to 35 nJ. Coupling efficiency into the nonlinear fiber was measured at around 10% and was not further optimized. Excitation conditions of PCF core were monitored with an infrared camera. Depending on spectral area, supercontinuum spectrum was recorded with Ocean Optics HR2000 and NIR512 spectrometers (coupled with a MM delivery fiber), or dispersed at a Zoltrix Omni λ-3000 monochromator and detected with a PbSe detector.

Numerical results were obtained with a model based on a split-step method solution to a nonlinear Schrödinger equation (NLSE). We used a model proposed by Travers *et al.* [12], which was extended to include wavelength-dependent loss of fiber. Raman parameterization

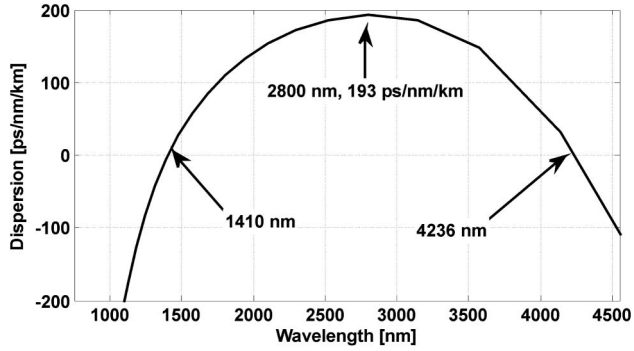

Fig. 3. Calculated dispersion profile of the fabricated PCF.

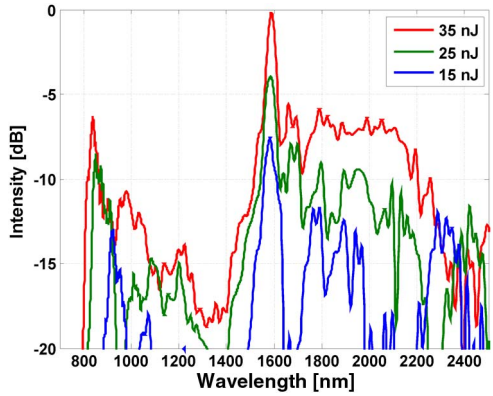

Fig. 4. Experimentally recorded supercontinuum spectra in the presented tellurite regular lattice PCF for incident pump pulse energy of 15, 25, and 35 nJ.

of NLSE was based on our experimental confirmation of location of peak Raman gain at $\Omega_R = 20.4$ THz in used tellurite glass labeled TWPN/I/6, and we assumed the remaining parameters similar to Price *et al.* [13].

Experimentally recorded supercontinuum spectra for incident pump pulse energies of 15, 25, and 35 nJ are shown in Fig. 4. The measured spectra were stable and fluctuated only with input-laser-intensity variations. All spectra were recorded in only a 2 cm long PCF sample. This was supported with a short nonlinear length scale of 0.3 mm and soliton fission length of 6 mm (order of soliton launched into fiber $N = 22$) calculated for the fiber, taking given experimental conditions (pump energy, coupling, pulse duration). These values allowed us to assume that spectral broadening would take place over the first few millimeters of propagation. We then preferred to reduce PCF length to limit the amount of lost soliton energy in the longer wavelength edge of spectrum. Supercontinuum spectrum recorded for the maximum pulse energy and simulated spectrum are both shown in Fig. 5. Supercontinuum covers a bandwidth from 800 to over 2500 nm, which is close to results obtained in ultrapure tellurite glass SC-PCFs [2,3] and in tellurite SC-PCFs with comparable attenuation, but pumped at longer wavelengths (1800–2000 nm) [6,7].

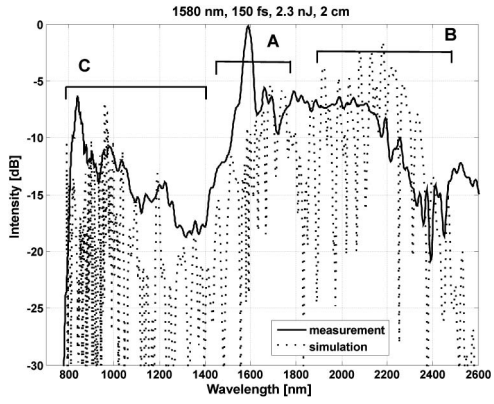

Fig. 5. Supercontinuum spectrum recorded experimentally in our regular-lattice tellurite PCF (solid line) and reconstructed numerically (dashed line). Capital letters mark corresponding components of numerically generated output temporal pulse-shape, shown in Fig. 6.

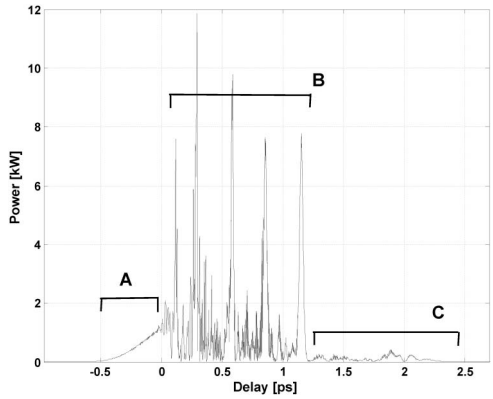

Fig. 6. Numerically generated temporal pulse-shape with capital letter markings corresponding to spectral components in Fig. 5.

Experimental spectrum is reconstructed with numerical model with good agreement. We believe the discrepancies, observable around the limits of the generated spectrum stem, from differences between physical dispersion of fiber and dispersion calculated from the SEM image of fiber, which in turn resulted from limited contrast between the air hole and glass as observed under our SEM microscope. Some unconverted energy of pump pulse, propagating in higher-order modes of fiber, was not reproduced numerically, either.

Figure 6 presents temporal pulse shape at the output of fiber with capital letters A, B, C in Figs. 5 and 6 representing corresponding spectral and temporal components. The proposed assignment is based on numerical spectrogram representation, shown together with the evolution of spectral broadening along the fiber in Fig. 7. After an initial stage of pulse compression corresponding to calculated soliton fission length of 6 mm, the trailing edge of pulse, redshifted due to anomalous dispersion, begins to break up into a train of solitons and a dispersive wave, blue shifted and delayed with respect to the pump pulse due to normal dispersion, is generated across the first ZDW (1410 nm). Spectral and temporal components marked with capital letters in Figs. 5 and 6 therefore are A: self-phase modulation; B: redshifting of solitons; C: dispersive wave.

The soliton train present in Fig. 6 and on the spectrogram in Fig. 7 comprises individual solitons with lengths of around $T_{\mathrm{sol}} = 30$ fs. Considering the first-order Raman shift of $\Omega_R = 20.4$ THz in our glass, redshift rate of the soliton self-frequency shift given by [14]

$$\frac{dv}{dz} = \frac{-0.09|\beta_2|\Omega_R}{2\pi T_{\mathrm{sol}}}, \tag{1}$$

yields shifts at the order of 16 THz/m. With a supercontinuum pump wavelength of 1580 nm, this corresponds to roughly 100 nm redshift over 2 cm of propagation, which does not explain the observed shift of roughly 700 nm (60 THz over 2 cm). Since four-wave mixing (FWM) can also give rise to solitons through modulation instability (MI) [12,15], we checked FWM phase-matching condition $\kappa = 0$, where the phase mismatch κ can be expressed as (e.g., [16])

$$\kappa = 2\gamma P_0(1 - f_R) + 2\sum_{m=1}^{\infty} \frac{\beta_{2m}}{(2m)!}\omega^{2m}, \tag{2}$$

and the resulting phase-matching curves are shown in Fig. 8. Group velocity dispersion (GVD) and quartic dispersion parameters for the developed PCF are both negative and equal -78×10^{-3} ps^2/m and -13×10^{-7} ps^4/m, respectively. This gives a limited bandwidth of about 400 nm for a Stokes-shifted parametric wavelength in a degenerate FWM process. Usually, this was considered fully supportive for the observed redshift of solitons [17]. It is to be noted, however, that soliton collisions [18], which were pointed out as often overlooked redshifting mechanisms [19,20], may also contribute to broadening, as in the case of our nonlinear fiber. As seen in spectrogram in Fig. 7, redshifting of solitons should take place between 1580 nm and roughly 2400 nm. In this wavelength range, anomalous dispersion is increasing, making each further redshifted soliton travel with a smaller group velocity along the fiber and also giving ample conditions for the energy exchange in direction from higher-frequency solitons, to lower-frequency solitons.

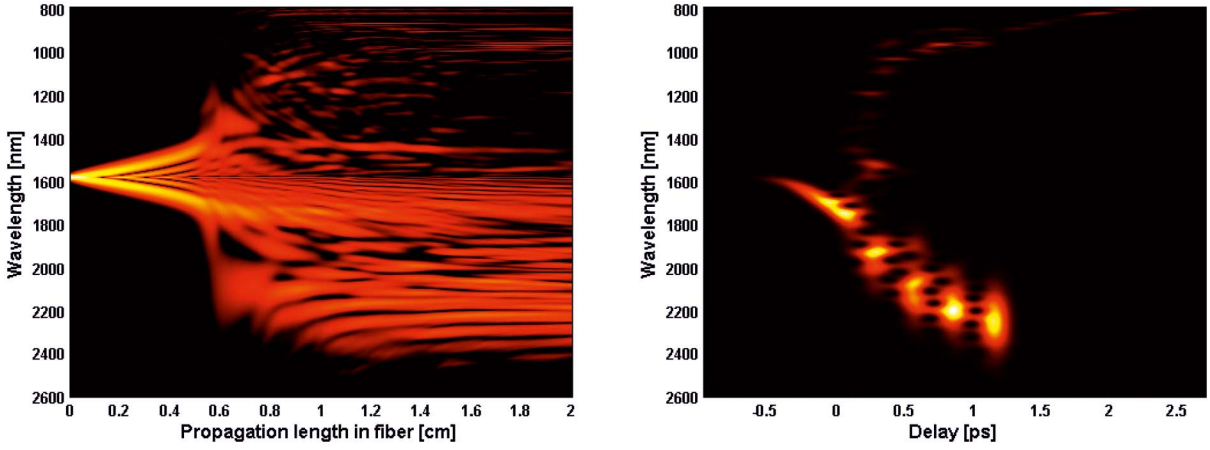

Fig. 7. Numerical reconstruction of evolution of spectrum along the PCF sample (right) and numerical spectrogram at the output of fiber (left).

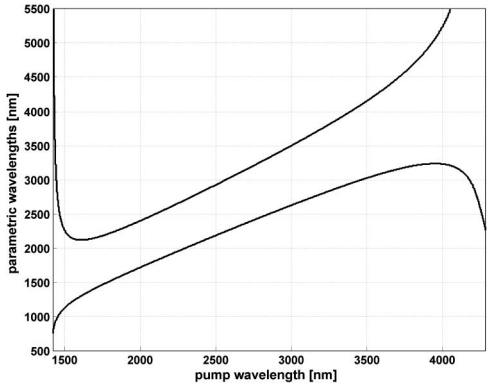

Fig. 8. FWM phase-matching curves calculated for input pulse energy of 2.3 nJ.

We have shown, for the first time to our best knowledge, that a regular, hexagonal lattice tellurite fiber can be successfully drawn with a stack-and-draw method without recrystallization to enable octave-spanning SG very close to the mid-infrared range. Pumping at 1580 nm enabled us to obtain a spectrum covering a bandwidth from 800 to 2500 nm, which is comparable to tellurite SC-PCFs pumped at 1800–2000 nm, or to results in ultrapure tellurite glass SC-PCFs. OH ion content in our glass resulted in relatively high attenuation, exceeding 10 dB/m at around 3000 nm, while in the covered spectral area it was below 5 dB/m (6.2 dB/m at 1550 nm in drawn fiber). A numerical model reproduced an experimental spectrum with good agreement. Calculations of soliton self-frequency shift rate indicated that this mechanism was insufficient to produce observed extent of soliton redshift in generated supercontinuum, in which FWM/MI-driven contributions as well as soliton collisions are possible. This was shown with calculated FWM phase-matching curves and a simple analysis of dispersion profile. Demonstrated fiber is a suitable platform for improvement in terms of modal properties and dispersion engineering, which would specifically enable more efficient FWM. Together with purification of OH impurity from glass, this should allow extending the spectrum further into the mid-infrared.

This work is supported by the Polish Ministry of Science and Higher Education research grant no. N515 523738 and the project operated within the Foundation for Polish Science Team Programme cofinanced by the European Regional Development Fund, Operational Program Innovative Economy 2007–2013.

References

1. P. Domachuk, N. A. Wolchover, M. Cronin-Golomb, A. Wang, A. K. George, C. M. B. Cordeiro, J. C. Knight, and F. G. Omenetto, Opt. Express **16**, 7161 (2008).
2. I. Savelii, O. Mouawad, J. Fatome, B. Kibler, F. Désévédavy, G. Gadret, J.-C. Jules, P.-Y. Bony, H. Kawashima, W. Gao, T. Kohoutek, T. Suzuki, Y. Ohishi, and F. Smektala, Opt. Express **20**, 27083 (2012).
3. I. Savelii, F. Desevedavy, J.-Ch. Jules, G. Gadret, J. Fatome, B. Kibler, H. Kawashima, Y. Ohishi, and F. Smektala, Opt. Mater. **35**, 1595 (2013).
4. M. Liao, X. Yan, G. Qin, C. Chaudhari, T. Suzuki, and Y. Ohishi, Opt. Express **17**, 15481 (2009).
5. G. Wang, T. Jiang, C. Li, H. Yang, A. Wang, and Z. Zhang, Opt. Express **21**, 4703 (2013).
6. X. Feng, W. H. Loh, J. C. Flanagan, A. Camerlingo, S. Dasgupta, P. Petropoulos, P. Horak, K. E. Frampton, N. M. White, J. H. V. Price, H. N. Rutt, and D. J. Richardson, Opt. Express **16**, 13651 (2008).
7. M. Liao, C. Chaudhari, G. Qin, X. Yan, C. Kito, T. Suzuki, Y. Ohishi, M. Matsumoto, and T. Misumi, Opt. Express **17**, 21608 (2009).
8. R. Stepien, R. Buczynski, D. Pysz, I. Kujawa, A. Filipkowski, M. Mirkowska, and R. Diduszko, J. Non-Cryst. Solids **357**, 873 (2011).
9. R. Stepien, R. Buczynskia, D. Pysz, and I. Kujawa, Proc. SPIE **8010**, 80100G (2011).
10. R. Stepien, R. Buczynski, D. Pysz, I. Kujawa, and M. Mirkowska, Photonics Lett. Pol. **2**, 16 (2010).
11. D. Lorenc, M. Aranyosiova, R. Buczynski, R. Stepien, I. Bugar, A. Vincze, and D. Velic, Appl. Phys. B **93**, 531 (2008).
12. J. C. Travers, M. H. Frosz, and J. M. Dudley, in *Supercontinuum Generation in Optical Fibers*, J. M. Dudley and R. Taylor, eds. (Cambridge University, 2010).
13. J. H. V. Price, T. M. Monro, H. Ebendorff-Heidepriem, F. Poletti, P. Horak, V. Finazzi, J. Y. Y. Leong, P. Petropoulos, J. C. Flanagan, G. Brambilla, X. Feng, and D. J. Richardson, IEEE J. Sel. Top. Quantum Electron. **13**, 738 (2007).
14. J. Herrmann and A. Nazarkin, Opt. Lett. **19**, 2065 (1994).
15. R. H. Stolen, E. P. Ippen, and A. R. Tynes, Appl. Phys. Lett. **20**, 62 (1972).
16. M. H. Frosz, T. Sørensen, and O. Bang, J. Opt. Soc. Am. B **23**, 1692 (2006).
17. S. M. Kobtsev and S. V. Smirnov, Opt. Express **13**, 6912 (2005).
18. M. N. Islam, G. Sucha, I. Bar-Joseph, M. Wegener, J. P. Gordon, and D. S. Chemla, J. Opt. Soc. Am. B **6**, 1149 (1989).
19. M. H. Frosz, O. Bang, and A. Bjarklev, Opt. Express **14**, 9391 (2006).
20. J. M. Dudley, G. Genty, and S. Coen, Rev. Mod. Phys. **78**, 1135 (2006).